Journal of Materials Chemistry C

Accepted Manuscript

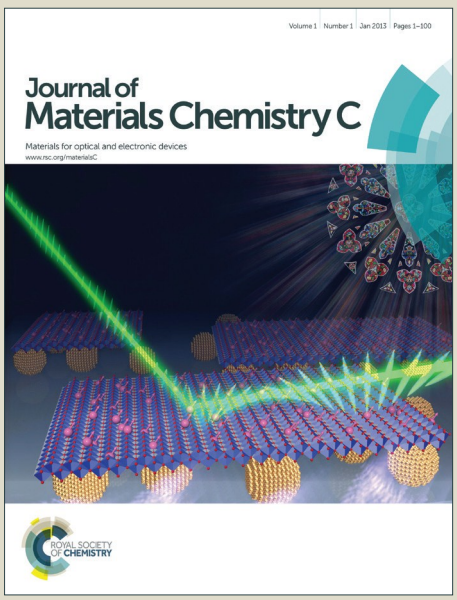

ROYAL SOCIETY OF CHEMISTRY

www.rsc.org/materialsC

Cite this: DOI: 10.1039/c0xx00000x

www.rsc.org/xxxxxx

ARTICLE TYPE

Structural transition in $KMnCrF_6$ – a chemically ordered magnetic ferroelectric.

Christina Drathen,*[a,c] Takeshi Nakagawa,[b‡] Wilson A. Crichton,[c] Adrian H. Hill,[c§] Yasuo Ohishi [d] and Serena Margadonna[b]

Received (in XXX, XXX) Xth XXXXXXXXX 20XX, Accepted Xth XXXXXXXXX 20XX
DOI: 10.1039/b000000x

The structure of the tetragonal tungsten bronze fluoride $KMnCrF_6$ was investigated via high-resolution synchrotron powder diffraction at variable temperatures (T = 5 – 950 K). A structural transition is observed at T = 400 K from a centrosymmetric high-temperature ($P4_2/mbc$) to an orthorhombic non-centrosymmetric phase ($Ccc2$). The phase transition is driven by the cooperative tilt of the MF_6 octahedra and displacements of Mn^{2+} and Cr^{3+} along the polar c-axis. The polar structure and the low temperature ferrimagnetic behaviour (T_N = 23 K) make $KMnCrF_6$ a potential multiferroic material. The room temperature orthorhombic structure is robust upon application of high-pressures up to 18 GPa with a bulk modulus K = 49.2(7) GPa.

Introduction

The tetragonal tungsten bronze (TTB) structural family comprises a large class of functional materials that adopt crystal structures related to the non-stoichiometric compound K_xWO_3. Magnéli elucidated the structure of the parent systems K_xWO_3 ($0.4 < x < 0.6$) more than sixty years ago and showed that they crystallize in the tetragonal space group $P4/mbm$, with $a_{TTB} \sim 12$ Å and $c_{TTB} \sim 4$ Å.[1] The prototype TTB structure that can be conveniently described as A_xBO_3, can be derived from the perovskite structure by a 45° rotation of a square group of four corner-sharing octahedral (Fig. 1). The resulting three-dimensional network contains square (**A1**), pentagonal (**A2**) and triangular (**C**) channels running parallel to the c-axis. The **A1** and **A2** sites are occupied by large mono- or divalent cations, whereas the **C** site remains vacant for all but small ions (e.g. Li^+). The stoichiometry varies between $A_{0.6}BO_3$ (vacant **C** sites) and $A_{0.4}BO_3$ (**C** and **A1** site vacant). Two structural building blocks are present: a perovskite type B_4O_{20} and a hexagonal B_3O_{15} unit (also called extra-perovskite). The irregular shape of the pentagonal channels is a result of the combination of these structural motifs: two angles are close to 90° and three close to 120°. A variety of chemical substitutions, both within the channels and/or the octahedral network, are possible and a large number of different compositions can be stabilized.

Indeed, the family of TTB oxides now comprises a large number of functional materials possessing a wide range of interesting and exploitable properties such as ferroelectricity, electro-optical and piezoelectricity.[2] The most prominent example is the well known ferroelectric $Ba_2NaNb_5O_{15}$ (BNN), which also shows non-linear optical properties.[3] At room temperature its average structure is reported as orthorhombic with polar symmetry $Cmm2$ (derived as a superstructure of the original TTB cell).[4] However, this corresponds only to a mean description of the atomic positions, as diffraction experiments on untwinned crystals revealed the presence of modulation satellites arising from octahedra distortion and tilting.[5] In addition, BNN displays a series of phase transitions as a function of temperature linked to ferroelectric and ferroelastic instabilities.[6,7] The exceptional physical properties of BNN fuelled extensive investigations on different TTB niobates leading to the discovery of a variety of new ferroelectrics and relaxor ferroelectrics.

Substitution of oxygen with fluorine is a very powerful tool to further extend the family of TTB materials as it offers access to a different range of transition metals with lower oxidation states and unpaired d-electrons. In addition, it affords the opportunity to couple ferroelectricity and magnetism within the same sublattice leading to potential multiferroic behaviour. Indeed, it has been

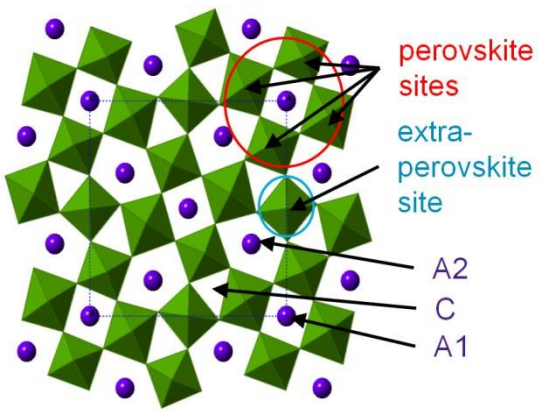

Fig. 1 Schematic representation of the prototype TTB structure. The two structural building blocks, a perovskite- and an extra-perovskite unit forming pentagonal (**A2**), square (**A1**) and triangular (**C**) channels are shown. The BO_6 site linking four perovskite B_4O_{20} units is herein referred to as the extra-perovskite site.

demonstrated experimentally that members of the TTB fluorides family such as $K_xFe^{2+}_xFe^{3+}_{1-x}F_3$ ($0.6 < x < 0.5$) are multiferroic at low temperatures and that the exact interplay between the different ordering parameters (ferroelectric, ferroelastic and magnetic) is finely tuned by subtle changes in compositions.[8]

The related TTB fluoride $KMnFeF_6$ has also been suggested to be multiferroic.[9] Even though ferroelectricity has not been directly measured, it adopts a polar structure typical of ferroelectric TTB bronzes, and it orders magnetically at low temperature.[10,11] $KMnFeF_6$ crystallizes in the acentric tetragonal space group $P4_2bc$.[10] The unit cell parameters show a doubling of the *c*-axis with respect to the fundamental TTB cell ($a \approx 12$ Å, $c \approx 2 \cdot c_{TTB} \approx 8$ Å).[10] The reported superstructure implies a charge-ordered pattern of Mn^{2+} and Fe^{3+} alternating around the perovskite cage, while the extra-perovskite site is statistically occupied by the two species.[10] One of the interesting features of $KMnFeF_6$ is that it shows frustrated magnetic order arising from the competition of antiferromagnetic (AF) superexchange interactions around the triangular channels. The magnetic structure consists of a non-collinear arrangement of the spins in the *ab*-plane. Consecutive planes along the *c*-axis order antiferromagnetically. The magnetic moments around the **C**-type channels adopt a star-like arrangement very close to the ideal 120° configuration, while all other interactions are unfrustrated leading to an anti-parallel alignment of the spins.[12] Magnetization measurements clearly revealed ferrimagnetic behaviour below the Néel temperature $T_N = 148$ K.[11] Recently, Nénert and Palstra have used symmetry analysis to assess the multiferroic properties of different fluorides.[9] Their work highlights $KMnFeF_6$ as a rare example of a ferrimagnetic compound exhibiting a strong interplay between magnetism and polarization below the magnetic ordering temperature. In addition, the application of a magnetic field should induce a change in the direction of the spontaneous polarization between the *c* and *b* crystallographic axis.

Several other TTB fluorides with general formula $KM^{2+}M^{3+}F_6$ have been reported (*M* = transition metal). These materials seem to adopt the same tetragonal $P4_2bc$ structure as $KMnFeF_6$ ($a \approx 12$ Å, c ≈ 8 Å) and order magnetically at low temperatures. The combinations studied to date include M^{2+}/M^{3+} (T_N): Zn/Ti (80 K); Zn/V (50 K); V/Sc (60 K); Cr/Sc (23 K); Mn/Sc (50 K), Fe/Co (110 K) and Mn/Cr (31 K).[13,14,15] Despite their intriguing behaviour, very little is known about this family of TTB fluorides. Only a few room temperature structural studies are available leaving many questions open. For instance, it would be important to follow the structural evolution as a function of temperature to reveal possible structural changes linked to tilt modulations, ionic/magnetic ordering and paraelectric-ferroelectric transitions. Also pressure is a powerful tool to investigate the relationship between strain (piezoelectricity) and spontaneous polarization (ferroelectricity); two properties which are linked by symmetry. The appearance of ferroelectricity in the TTB fluorides has been connected to an orthorhombic phase, which may be suppressed at high-pressures.

These type of studies are fundamental to achieve a deeper understanding of the interplay between the different ordering phenomena and to assess the multiferroic behaviour. It is highly desirable to work with different transition metal combinations in order to achieve chemical control of the different ferroic ordering parameters in TTB fluorides. Phenomena such as charge ordering and/or Jahn-Teller (JT) distortions that further complicate the structures of homometallic compounds such as K_xMF_3 (*M* = V, Cr, Mn, Fe) can be circumvented by combining two non-JT active metals. Whilst this approach is not aimed at optimising the material's properties, it will provide fundamental insight into the structure-property relationships of this type of compounds. These considerations have motivated us to initiate a systematic investigation of the structural phase diagram of the related compound $KMnCrF_6$. Our choice to study $KMnCrF_6$ has been driven by the evident similarities with $KMnFeF_6$: both systems contain magnetically active cations on all sites and the M^{2+}/M^{3+} ionic radii ratio remains unchanged ensuring minimum disruption of the ionic order pattern. However, changing the chemical nature of the M^{3+} cation could result in a different magnetic response. Unlike $KMnFeF_6$, $KMnCrF_6$ should show a predominant ferromagnetic (FM) behaviour if we consider the number and geometries of the different magnetic exchange pathways. The larger magnitude of polarization obtainable in ferromagnets as compared to antiferromagnets is desirable from an application point of view.[16]

In this work, we report the results of a detailed investigation of the structural and magnetic properties of the TTB fluoride $KMnCrF_6$. Synchrotron X-ray powder diffraction measurements were performed between 5 and 950 K and showed the onset of a structural phase transition at $T_S = 400$ K. The high temperature structure ($T \geq 400$ K) was determined to be tetragonal with centric symmetry $P4_2/mbc$. In contrast to what has been previously reported,[13] between 5 and 400 K, $KMnCrF_6$ crystallizes in a orthorhombically distorted polar variant (space group *Ccc*2) of the tetragonal $P4_2bc$ supergroup. The distortion is linked to the cooperative tilting of the MF_6 octahedra and the displacement of the transition metal cations away from the centre of the octahedra. The orthorhombic structure also supports full chemical order on all crystallographic sites. Room temperature high-pressure powder diffraction experiments showed that the *Ccc*2 structure remains robust up to $p = 18$ GPa with the orthorhombic distortion increasing upon pressurization. Finally, magnetization measurements revealed the onset of ferrimagnetic order at $T_N = 23$ K.

These results clearly indicate that $KMnCrF_6$ has a much richer phase diagram than previously expected where many different ordering parameters (ionic, ferroelectric and magnetic) coexist. Our analysis strongly indicates that the phase transition observed at 400 K corresponds to a change from an apolar to a polar structure. It is therefore very likely that such transition corresponds to a paraelectric-ferroelectric crossover and that $KMnCrF_6$ displays multiferroic properties below the magnetic transition.

Experimental Section

Polycrystalline samples of $KMnCrF_6$ of light green colour were obtained via solid-state synthesis from stoichiometric mixtures of KF, MnF_2 and CrF_3 (at least 99.9 % purity). All sample manipulations were performed inside a glove box under inert argon atmosphere. The pelletized reactants were contained in a well-clamped gold tube and heated to 750°C for 72 hours. The

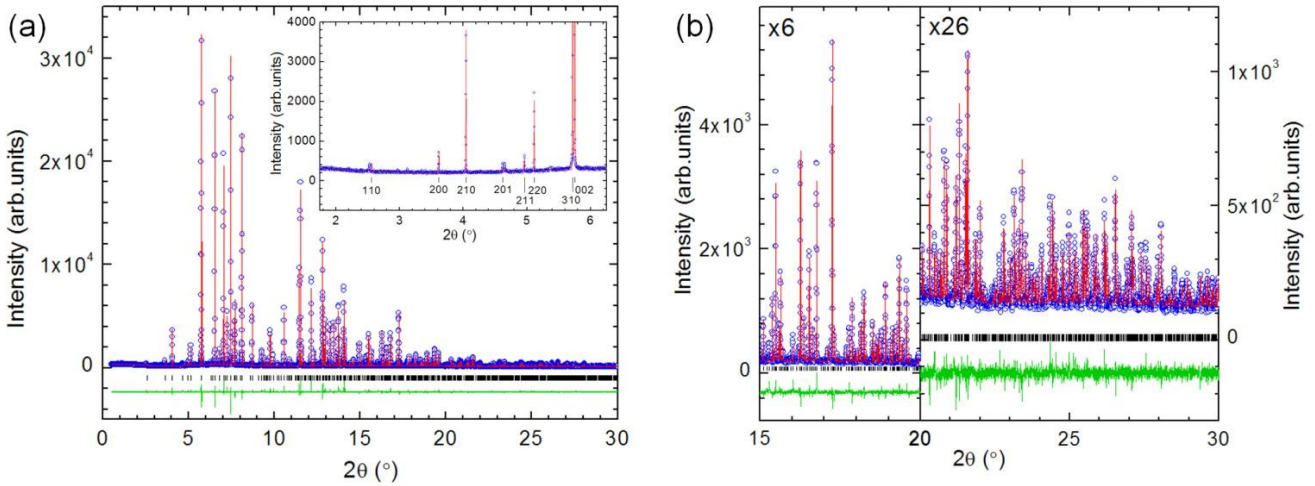

Fig. 2 (a) Final observed (open blue circles), calculated (red line) and difference (green line) synchrotron X-ray powder diffraction profile of $KMnCrF_6$ (space group $P4_2/mbc$), collected on ID31 (ESRF), λ = 0.39992 Å, T = 423 K. The lower solid green line shows the difference profiles and the tick marks show the reflection positions. (Inset a) The low 2θ region highlights the superlattice reflections (2 0 ½) and (2 1 ½) that indicate a doubling of the c-axis with respect to the conventional TTB cell. (b) Magnification of the high 2θ region.

gold capsules was either sealed in a quartz tube under reduced argon pressure (sample I) or kept under nitrogen flow (sample II) for the duration of the heat treatment. The stoichiometry of sample I was confirmed to be $KMnCrF_6$ by ICP elemental analysis (K, 13.7(2) %; Mn, 19.5(2) %; Cr, 20.7(2) %; F, 46(1) %.) Incorporation of nitrogen in sample II was ruled out by CHNS elemental analysis.

Synchrotron X-ray diffraction experiments were performed on beamlines ID31 and ID11 ESRF, France. The samples were sealed in 0.5 mm diameter thin-wall glass or quartz capillaries. Diffraction profiles of sample I were recorded between T = 5 – 823 K on beamline ID31 (λ = 0.39992 Å). The data were binned in the 2θ range 0.1 – 48° to a step of 0.002° 2θ. Diffraction profiles of sample II were collected on ID11 (λ = 0.42 Å) between T = 300 – 950 K. The data were collected on a Frenlon2k camera and integrated with Fit2D in the 2θ range 1.8 – 26.2° with a step of 0.014° 2θ.

High-pressure synchrotron X-ray diffraction experiments were performed on beamline BL10XU, SPring-8, Japan. The powder (sample I) together with a small ruby chip was loaded in a diamond anvil cell; helium was used as a pressure transmitting medium. The applied pressure was measured immediately after exposure by the ruby fluorescence method without dismounting the cell. The diffraction patterns (λ = 0.41338 Å) were collected at room temperature between 0.2 and 18 GPa. Data were recorded using a flat image plate detector and integrated using WinPIP.[17] Analysis of all diffraction data was carried out with the GSAS suite of Rietveld programs.[18,19]

DC magnetization data of sample I were measured on a Quantum Design MPMS magnetometer. The temperature dependence of magnetization was determined under applied magnetic fields H = 0.01, 0.1, 1 T. Magnetic hysteresis loops up to 1 T were collected at 5 K.

Results

The high-temperature structure

The high-resolution synchrotron X-ray powder diffraction profiles collected in the temperature range between 423 and 823 K on $KMnCrF_6$ can be readily indexed considering a tetragonal cell with symmetry $P4_2bc$. The presence of Bragg reflections with Miller indexes (2 0 ½) and (2 1 ½) clearly indicate the doubling of the c-axis compared to the fundamental TTB structure. These super-lattice peaks (inset Fig. 2) are visible throughout the entire temperature range measured. Detailed Rietveld refinements of the 423 K data were then initiated using a model based on the reported structure of $KMnFeF_6$ where the Mn^{2+} and Cr^{3+} ions are ordered around the perovskite cage while the extra-perovskite site is statistically occupied by the two species. The refined lattice constants are $a_{TTB} \approx a$ = 12.67146(1) Å and $2 \cdot c_{TTB} \approx c$ = 7.96514(1) Å. Occupancies of Mn^{2+} and Cr^{3+} on the two perovskite-type sites (8c), as well as the pentagonal **A2** site hosting K^+ (8c), refined to $Occ.$ = 1 within error, and were therefore fixed to unity. The total occupancy of the mixed extra-perovskite type site (4b) was constrained to be equal to one, with a 1:1 ratio of Mn:Cr, in agreement with the elemental analysis. The ~~s~~quare **A1** channels (4a) are only partially filled. The refined M-F bond distances (R_i) tabulated in Table 2 were used to calculate the individual bond-valences (v_i) according to the expression:

$$v_i = \exp((R_0 - R_i)/b),$$

where R_0 is a tabulated value for the specific bond type and metal valence state and b is an empirical constant typically equal to 0.37 Å. [20, 21] The site's valence (*i.e.* the bond valence sum, BVS) is the sum of v_i. Inspection of the refined M-F (M = transition metal) bond distances and BVS confirmed the suggested ionic ordered pattern. The mean values of the distances corresponding to the two perovskite type sites (8c) are 2.094(6) Å and 1.925(6) Å clearly indicating full occupation of the two sites by Mn^{2+} (high-spin, BVS 2.067) and Cr^{3+} (BVS 2.778), respectively. The average value of 1.975(7) Å and the deviation of the BVS for Mn^{2+} and Cr^{3+} states on the extra-perovskite site support a mixed occupancy by the divalent and trivalent species.

Table 1 Rietveld refinement results at 423 K.[a]

space group: $P4_2/mbc$ No. 135				T = 423 K	
a = 12.68202(1) Å, c = 7.97617(1) Å,				V = 1282.837(2) Å^3	
		x	y	z	B_{iso}/ Å^2
Mn1	4*c*	0	0.5	0	0.77(3)
Cr1	4*c*	0	0.5	0	0.77(3)
Mn2	8*h*	0.0737(2)	0.7865(2)	0	0.76(4)
Cr2	8*h*	0.4250(2)	0.2894(2)	0.5	0.63(4)
K1	8*g*	0.8280(1)	0.6720(1)	0.75	3.28(4)
K2	4*b*	0	0	0.75	1.13(6)
F1	8*h*	0.5663(5)	0.3477(4)	0	2.50(3)
F2	8*h*	0.9267(5)	0.8651(4)	0.5	2.50(3)
F3	8*h*	0.7850(4)	0.2738(4)	0	2.50(3)
F4	8*h*	0.4953(4)	0.1553(5)	0	2.50(3)
F5	8*h*	0.9808(4)	0.6534(6)	0.5	2.50(3)
F6	4*d*	0	0.5	0.75	2.50(3)
F7	16*i*	0.2091(2)	0.0763(2)	0.7409(6)	2.50(3)

[a] wR_p = 8.22 %; R_p = 6.33 %

Table 2 *M*-F distances and bond valence sums (BVS) at 423 K.

Mn1/Cr1-F	*d*/ Å	Mn1/Cr1-F	*d*/ Å
Mn1/Cr1-F4	1.970(7)	Mn1/Cr1-F5	1.961(7)
Mn1/Cr1-F4	1.970(7)	Mn1/Cr1-F6	1.994
Mn1/Cr1-F5	1.961(7)	Mn1/Cr1-F6	1.994
average	1.975(7)	BVS(Mn^{2+})	2.840
		BVS(Cr^{3+})	2.428

Mn2-F	*d*/ Å	Mn2-F	*d*/ Å
Mn2-F1	2.117(6)	Mn2-F5	2.058(6)
Mn2-F2	2.114(7)	Mn2-F7	2.068(4)
Mn2-F3	2.136(6)	Mn2-F7	2.068(4)
average	2.094(6)	BVS(Mn^{2+})	2.067

Cr2-F	*d*/ Å	Cr2-F	*d*/ Å
Cr2-F1	1.938(7)	Cr2-F4	1.920(7)
Cr2-F2	1.901(6)	Cr2-F7	1.922(4)
Cr2-F3	1.948(6)	Cr2-F7	1.922(4)
average	1.925(6)	BVS(Cr^{3+})	2.778

[a] Mn1/Cr1 reside on the 4*c* site, Mn2 and Cr2 are on 8*h* sites

In order to check the symmetry assignment to the polar space-group $P4_2bc$, we searched for the existence of pseudosymmetry with respect to higher-symmetry structures. Generally, the search of possible higher symmetry is limited to the minimal supergroups of the original space group. Two structures can be pseudosymmetric if the atomic displacements that allow transformation of the lower symmetry into the higher symmetry variant, are smaller than an arbitrarily assigned threshold value (say, ~2 Å). Pseudosymmetry evaluation based on this atomic displacement method has been extensively used by Abrahams to predict new ferroelectrics and to assess false symmetry assignment of polar structures, see for example references (22, 23). Abrahams structural criteria are as follows: (i) values of atomic displacements < 0.1 Å are a strong indication of wrong symmetry assignment and the real structure should be described in the higher symmetry configuration and (ii) the atomic displacements along the polar axis relating the lower and higher symmetry structures have to be < 1 Å for a phase transition to occur at high temperature (e.g. paraelectric-ferroelectric transition).[24,25] These criteria were used to predict ferroelectricity and ferroelasticity in the related TTB fluoride $K_{0.6}Fe^{2+}_{0.6}Fe^{3+}_{0.4}F_3$.[22]

The pseudosymmetry search for $KMnCrF_6$ and the evaluation of the atomic displacements were performed with the program PSEUDO available on the Bilbao Crystallographic Server.[26] The initial atomic positions used were those obtained from the Rietveld refinement of the 423 K data in space group $P4_2bc$ (Table S1). The results clearly indicate that within the tolerance value for maximum atomic displacement of 2 Å, the $P4_2bc$ structure of $KMnCrF_6$ has $P4_2/mbc$ pseudosymmetry. The calculated atomic displacements along the polar *c*-axis, *d*(*z*), that relate the two variants are generally very small (< 0.1 Å) for all the metal cations (Table S2). Following Abrahams' criteria, it is very likely that the real structure of $KMnCrF_6$ at 423 K has symmetry $P4_2/mbc$. Rietveld refinements were then repeated in space-group $P4_2/mbc$ (Fig. 2). It is expected that the difference in the refinements using the two centric and acentric variants would be rather small. Indeed, the fitting statistics change only slightly even though the number of refined positional parameters is approximately halved ($P4_2bc$: χ^2 = 1.947, wR_p = 7.88 %; R_p = 6.00 %; $P4_2/mbc$: χ^2 = 2.113, wR_p = 8.22 %; R_p = 6.33 %). Results of the final refinement in the centric space group $P4_2/mbc$ are summarized in Table 1. The ionic ordered pattern is maintained and the average *M*-F distances are essentially identical to those obtained in the lower symmetry setting (Table 2).

The room-temperature structure

Inspection of the diffraction profiles of $KMnCrF_6$ readily identified that cooling from 423 K to room temperature induces a subtle structural distortion. This is reflected by the broadening and/or splitting of selected Bragg reflections, including those with Miller indices (*hh*0) (Fig. 3(a)). This type of behaviour is typical of a monoclinic distortion of the original tetragonal unit cell that can be conveniently described in an orthorhombic setting. The unit cell parameters of the orthorhombic supercell a_O and b_O lie along the basal plane diagonals of the original tetragonal cell: $a_O \approx a_{TTB}\cdot\sqrt{2}$, $b_O \approx a_{TTB}\cdot\sqrt{2}$. This conversion automatically leads to a change in centring from $P \rightarrow C$ and a doubling of the unit cell volume (Fig. 3(b)). Of the subgroups of $P4_2/mbc$, only *Cccm* describes the observed splitting of the (*hh*0) reflections. Since the structure of $KMnCrF_6$ was previously reported to be acentric,[13] subgroups of $P4_2bc$ were considered for the symmetry assignment. *Ccc*2 is a subgroup of both $P4_2bc$ and *Cccm* and perfectly describes the observed distortion. Rietveld refinements of the room-temperature data were then initiated using structural models with *Ccc*2 symmetry (Fig. 4). The lattice constants refined to a_{Ccc2} = 17.90002(3) Å, b_{Ccc2} = 17.88804(3) Å, c_{Ccc2} = 7.93839(1) Å. The small difference between the *a* and *b* lattice parameters clearly show that the distortion is very small with an orthorhombic strain parameter of 6.7×10^{-4} indicating that the unit cell is metrically pseudotetragonal.

In the course of the refinements, occupancies were fixed to unity except for the potassium residing in the square channels. The refined composition $K_{1.033(3)}MnCrF_6$ is in good agreement with the results of the high-temperature refinement and of the elemental analysis. It was not possible to refine all atomic positions simultaneously due to correlations; the coordinates of Mn, Cr, F and K(1, 2) were refined together, but separately from K(3, 4). Temperature factors of all atoms were refined simultaneously. The results of the Rietveld refinements are summarized in Table 3 (wR_p = 8.67 %; R_p = 5.98 %).

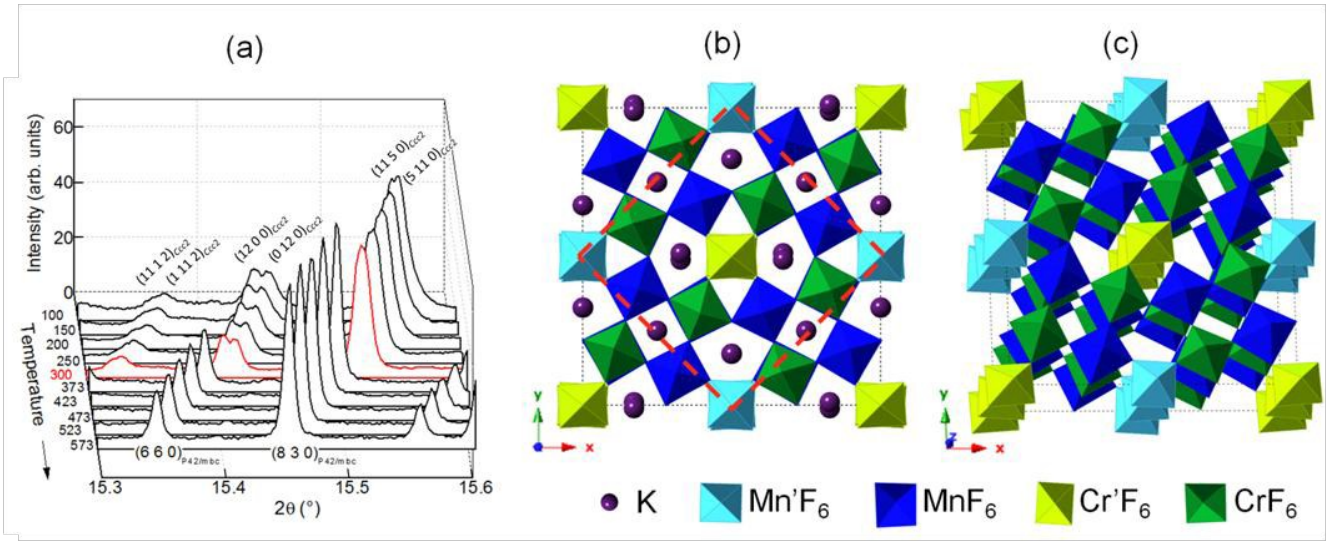

Fig. 3 (a) Diffraction profiles collected at variable temperature show the splitting of the $(660)_T$ reflection at $T \leq 300$ K (red line). The splitting can be indexed as (12 0 0), (0 12 0) in the orthorhombic space group *Ccc*2. (b) The *Ccc*2 cell adopted by $KMnCrF_6$ at 300 K seen along the *c*-axis. Mn' and Mn correspond to Mn/Cr1 on the extra-perovskite site (4*b*) and to Mn2, Mn3 on the perovskite sites (8*d*), respectively. Cr' and Cr correspond to Mn/Cr2 on the extra-perovskite site (4*a*) and to Cr2, Cr3 on the perovskite sites (8*d*), respectively. The high-temperature $P4_2/mbc$ cell is outlined by the dashed red line. (c) Tilted view of the *Ccc*2 cell, highlighting the alternating order of MnF_6 and CrF_6 octahedra on the perovskite site, and the hypothetical columns of MnF_6 and CrF_6 on the extra-perovskite sites. K^+ was omitted for clarity.

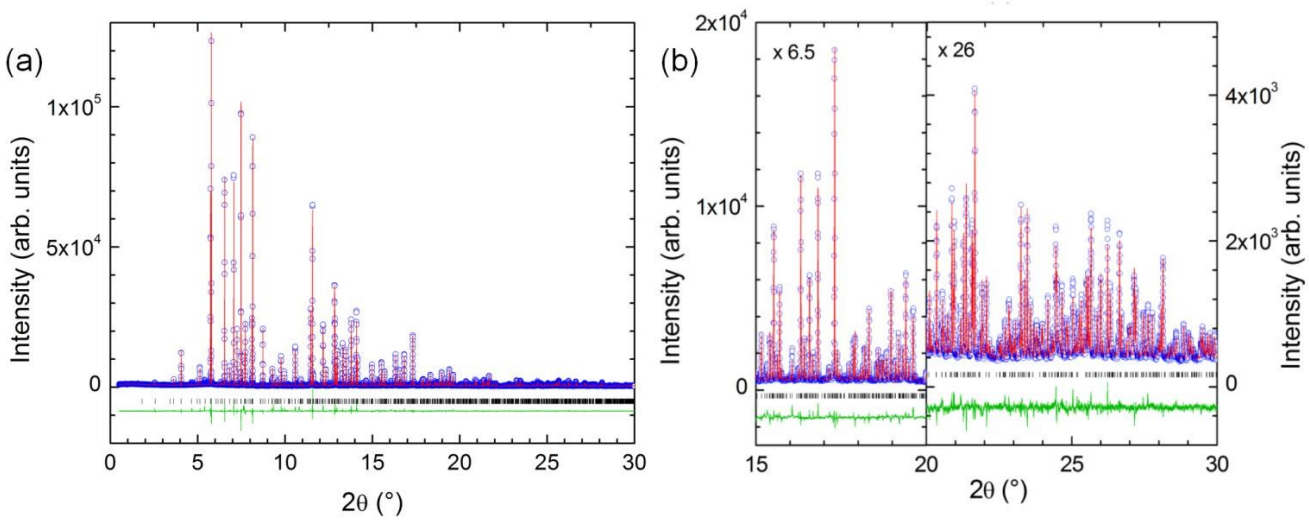

Fig. 4 (a) Observed (open blue circles), calculated (red line) and difference (green line) synchrotron powder diffraction Rietveld profile of $KMnCrF_6$ (space group *Ccc*2), collected at ID31, $\lambda = 0.39992$ Å, $T = 300$ K. (b) Magnification of the high 2θ region.

A pseudosymmetry search was initiated following the same method already described in the previous paragraph. As before, the results proposed that, at room temperature, the *Ccc*2 structure of $KMnCrF_6$ has *Cccm* pseudosymmetry. This time, however, the atomic displacements along the polar *c*-axis are uniformly larger than $d(z) > 0.1$ Å for all the metals (Table S3). The distortions of Mn and Cr from the high-symmetry structure are much more pronounced, providing a good indication that at room temperature the structure is likely acentric with *Ccc*2 symmetry. The values of the atomic displacements are also small enough to envisage a possible phase transition to a non-polar configuration of higher symmetry with increasing temperatures. Different empirical relationships have been developed to correlate $d(z)$ and the transition (Curie) temperature T_C. For instance Kroumova *et al.* [25] proposed the following formula:

$$T_C = \alpha \cdot (d(z)_{max} - d(z)_{min})^2 + \beta$$

where $d(z)_{max}$ and $d(z)_{min}$ are the values of the maximal and the minimal displacements along the polar axis, $\alpha = 0.22(4) \times 10^4$ K Å^{-2} and $\beta = T$(experiment). Using the maximum displacement $d(z)$ of 0.19 Å obtained for Cr1 we can estimate a $T_C \sim 380$ K.

The tetragonal to orthorhombic (T→O) structural phase

Table 3 Rietveld refinement results at 300 K.[a]

space group: *Ccc*2		No. 37		T = 300 K		
a = 17.90002(3) Å		b = 17.88804(3) Å		c = 7.93839(1) Å		
V = 2541.842(5) Å^3						
		x	y	z	B_{iso}/ Å^2	*Occ.*
Mn/Cr1	4*b*	0	0.5	0.520(2)	0.44(4)	1
Mn/Cr2	4*a*	0	0	0.024(2)	0.65(5)	1
Mn2	8*d*	0.8925(5)	0.8196(4)	0.519(2)	0.44(4)	1
Mn3	8*d*	0.1813(4)	0.3936(5)	0.020(2)	0.44(4)	1
Cr2	8*d*	0.8927(5)	0.8195(5)	0.019(2)	0.65(5)	1
Cr3	8*d*	0.1821(5)	0.3936(5)	0.518(2)	0.65(5)	1
K1	8*d*	1.0008(3)	0.6724(2)	0.268(2)	2.21(3)	1
K2	8*d*	0.3284(2)	0.4896(2)	0.769(2)	2.21(3)	1
K3	4*c*	0.25	0.25	0.765(2)	0.94(5)	0.523(7)
K4	4*c*	0.25	0.25	0.266(2)	0.94(5)	0.644(7)
F1	8*d*	0.997(1)	0.7811(4)	0.014(4)	2.17(3)	1
F2	8*d*	0.2217(4)	0.497(2)	0.502(3)	2.17(3)	1
F3	8*d*	0.924(1)	0.923(1)	0.985(3)	2.17(3)	1
F4	8*d*	0.079(1)	0.424(1)	0.497(3)	2.17(3)	1
F5	8*d*	0.086(1)	0.933(1)	0.003(3)	2.17(3)	1
F6	8*d*	0.071(1)	0.585(1)	0.505(3)	2.17(3)	1
F7	8*d*	0.290(1)	0.358(1)	0.007(3)	2.17(3)	1
F8	8*d*	0.642(1)	0.790(1)	0.487(2)	2.17(3)	1
F9	8*d*	0.855(1)	0.717(1)	0.996(2)	2.17(3)	1
F10	8*d*	0.282(1)	0.355(1)	0.512(3)	2.17(3)	1
F11	8*d*	0.8946(5)	0.8081(5)	0.256(4)	2.17(3)	1
F12	8*d*	0.1665(4)	0.3883(4)	0.755(4)	2.17(3)	1
F13	8*d*	0.8979(6)	0.8105(5)	0.767(5)	2.17(3)	1
F14	8*d*	0.1849(5)	0.3900(5)	0.268(5)	2.17(3)	1
F15	4*a*	0	0	0.256(5)	2.17(3)	1
F16	4*b*	0	0.5	0.745(3)	2.17(3)	1

[a] wR_p = 8.67 %; R_p = 5.98 %.

transition described above doubles the number of crystallographic sites, which could have strong implications on the charge-ordering pattern. Very importantly, it generates two distinct extra-perovskite sites (4*a* and 4*b*), supporting additional Mn^{2+}/Cr^{3+} order. Occupation of the 4*a* and 4*b* positions by only one type of metal ion (Mn^{2+} or Cr^{3+}) would result in columns of MnF_6 and CrF_6 octahedra running along the *c*-axis, which is unlikely considering the local strains that would arise from stacks of smaller CrF_6 and larger MnF_6 octahedra. On the other hand, the alternating order of Mn^{2+} and Cr^{3+} around the perovskite unit is the same as in the high-temperature structure. The distinction between different ordering motifs is difficult with X-ray data, given that the Mn^{2+} and Cr^{3+} scattering lengths are very similar. The *M*-F bond distances and BVS are, however, more selective and Mn2, Mn3, Cr2 and Cr3 (8*d*) agree well with an ordered perovskite site (Table 4). While Mn2 and Mn3 with BVS of 2.24 and 2.29 correspond well to Mn^{2+}, the BVS for Cr2 and Cr3 (2.54 and 2.59, respectively) are slightly lower than expected for Cr^{3+}. The values of the distances relative to the transition metals residing on the fourfold extra-perovskite positions are intermediate implying simultaneous occupation by both types of ions.

We note that trial refinements starting from statistically occupied extra-perovskite sites showed only a preferential occupation (~75 %) of Mn^{2+} and Cr^{3+} on (4*b*) and (4*a*) sites, respectively. These results demonstrate that the ionic ordering pattern of $KMnCrF_6$ at ambient conditions is analogous to that described for the high-temperature $P4_2/mbc$ phase.

Structural evolution as a function of temperature

The evolution of the diffraction profiles collected on warming

Table 4 *M*-F distances and bond valence sums (BVS) at 300 K.[a]

Mn/Cr1-F	*d*/ Å	Mn/Cr1-F	*d*/ Å
Mn/Cr1-F4	1.98(2)	Mn/Cr1-F6	1.98(2)
Mn/Cr1-F4	1.98(2)	Mn/Cr1-F16	1.78(3)
Mn/Cr1-F6	1.98(2)	Mn/Cr1-F16	2.19(3)
average	1.98(2)	BVS(Mn^{2+})	2.93
		BVS(Cr^{3+})	2.51
Mn/Cr2-F	*d*/ Å	Mn/Cr2-F	*d*/ Å
Mn/Cr2-F3	1.97(2)	Mn/Cr2-F5	1.95(2)
Mn/Cr2-F3	1.97(2)	Mn/Cr2-F15	1.84(4)
Mn/Cr2-F5	1.95(2)	Mn/Cr2-F15	2.12(4)
average	1.97(3)	BVS(Mn^{2+})	2.97
		BVS(Cr^{3+})	2.54
Mn2-F	*d*/ Å	Mn2-F	*d*/ Å
Mn2-F1	2.10(2)	Mn2-F10	2.08(2)
Mn2-F5	2.07(2)	Mn2-F11	2.10(3)
Mn2-F8	2.07(2)	Mn2-F13	1.97(4)
average	2.07(3)	BVS(Mn^{2+})	2.24
Mn3-F	*d*/ Å	Mn3-F	*d*/ Å
Mn3-F2	2.09(3)	Mn3-F9	2.09(2)
Mn3-F6	2.02(2)	Mn3-F12	2.18(3)
Mn3-F7	2.06(2)	Mn3-F14	1.97(4)
average	2.07(3)	BVS(Mn^{2+})	2.29
Cr2-F	*d*/ Å	Cr2-F	*d*/ Å
Cr2-F1	1.98(2)	Cr2-F9	1.96(2)
Cr2-F3	1.95(2)	Cr2-F11	1.90(3)
Cr2-F7	1.96(2)	Cr2-F13	2.01(4)
average	1.96(3)	BVS(Cr^{3+})	2.54
Cr3-F	*d*/ Å	Cr3-F	*d*/ Å
Cr3-F2	1.99(3)	Cr3-F10	1.92(2)
Cr3-F4	1.92(2)	Cr3-F12	1.91(3)
Cr3-F8	2.00(2)	Cr3-F14	1.98(4)
average	1.95(3)	BVS(Cr^{3+})	2.59

[a] Mn/Cr1 and Mn/Cr2 reside on the 4*a* and 4*b* site, Mn2, Mn3, Cr2 and Cr3 on 8*d* sites.

between 423 and 823 K on ID31 shows that $KMnCrF_6$ remains strictly tetragonal with both lattice constants, *a* and *c* increasing smoothly for the entire temperature range. The rate of expansion in this temperature range is quite anisotropic at 0.021 and 0.011 ppm K^{-1} for the *a* and *c* lattice constants, respectively. As previously discussed, at room temperature $KMnCrF_6$ adopts an orthorhombically distorted structure, which is robust on cooling down to 5 K. The rate of contraction of the basal plane lattice constants between $5 \leq T \leq 300$ K is substantially isotropic with the orthorhombic strain parameter remaining essentially constants throughout the temperature range with a calculated value of 4.6×10^{-4} at 5 K (a_{Ccc2} = 17.8540(1) Å, b_{Ccc2} = 17.8457(1) Å, c_{Ccc2} = 7.89452(2) Å, Figure S1). Figure 5 shows the temperature dependence of lattice constants and volume between $5 \leq T \leq 823$ K. While the *a*- and *b*-axis expand smoothly throughout the entire temperature range, a distinctive change is observed for the *c*-axis at temperatures between 423 and 373 K. This discontinuity can be understood if we consider that one of the consequences of the T→O transition is a significant increase in octahedra distortion with the tilting angles deviating significantly from 180°. Such distortion is readily observable in the abrupt contraction of the *c*-axis that can therefore be taken as a distinctive signature of the transition.

In order to determine the T→O transition temperature more

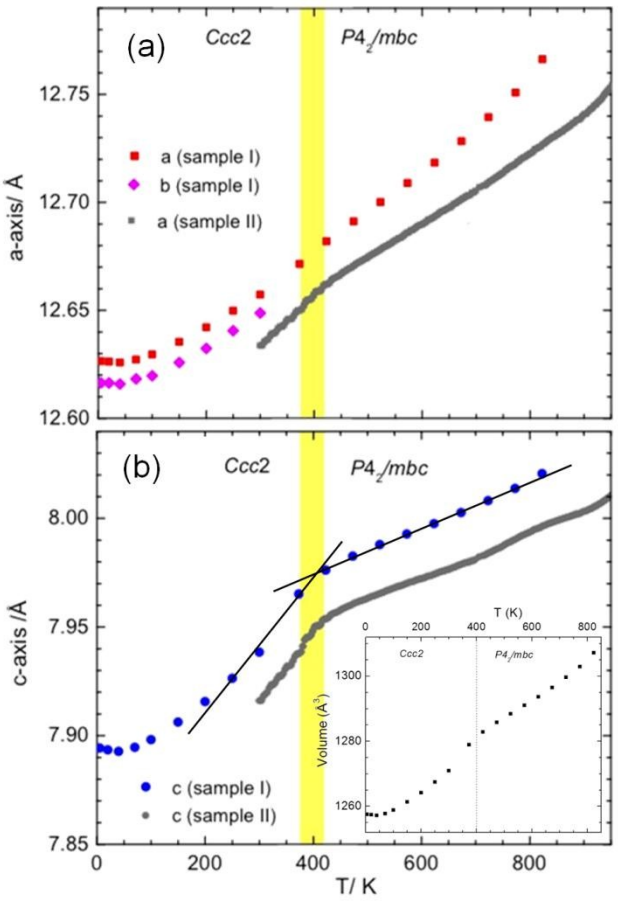

Fig. 5 The temperature dependence of the lattice parameters of sample I and II of $KMnCrF_6$ derived from Rietveld refinements of powder diffraction data collected on beamlines ID31 and ID11, respectively (a) The *a*-, *b*- and (b) *c*-axis of sample I and II of $KMnCrF_6$ shows good agreement between samples, although the absolute values vary due to slight changes in composition. The lattice parameters of the orthorhombic cell have been converted to the tetragonal setting, $a' = a_O/\sqrt{2}$. The change in slope of the *c*-axis is connected to the O→T phase transition.(inset) The unit cell volume as a function of temperature. Notice, curvature changes at the highest temperatures are related to the eventual oxidation of the sample as the capillary was destroyed.

precisely, the lattice constants of sample II were followed on beamline ID11 (ESRF) between 300 and 950 K (Fig. 5). The lower resolution of the data does not allow to resolve the subtle orthorhombic splitting. However, the gain in temperature resolution more than made up for this. Therefore, Rietveld refinements were performed in space group $P4_2bc$ ($c_{Ccc2} = c_{P42bc}$) considering that the choice of lattice metrics has no influence on the thermal evolution of the *c*-axis parameter. Although the absolute values of the lattice parameters of the two samples are not identical, their temperature evolution is analogous with a discontinuity clearly visible on the *c*-axis of sample II at 400 K. The small difference in volume is probably related to a slight variation in composition which has no apparent effect on the onset of the structural phase transition which can then be placed at T_S = 400 K.

Structural evolution as a function of pressure

Synchrotron X-ray powder diffraction profiles of $KMnCrF_6$ were collected on the high-pressure beamline BL10XU (SPring-8, Japan) at room temperature between 0.2 and 18 GPa. Rietveld refinements of the data were undertaken using the orthorhombic *Ccc*2 model, leading to values of the lattice constants: a_{Ccc2} = 17.8645(4) Å, b_{Ccc2} = 17.8615(5) Å, c_{Ccc2} = 7.79176(5) Å, at 0.19 GPa; with background-subtracted R_p = 3.3 % and wR_p = 6.07 %. Rietveld refinements at selected pressures are shown in Figure 6. The pressure evolution of the reduced lattice metrics is shown in Figure 7, together with 3rd order Birch-Murnaghan equations of state (EoS) fitted to the weighted *p* and lattice parameter data.

The data were fitted over the pressure range up to and including our datum at 12.11 GPa, using the program Eosfit.[27] Through inspection of the pressure mis-fits to subsets of the data, it was evident that higher-pressure data were probably affected by strain from grain-grain contact. We also note that these higher pressures coincide with the solidification of He.

Fitting the EoS parameters to the 19 available *p*, *V* data resulted in a V_0 = 2536.1(6) Å^3, an isothermal bulk modulus, $K_{T,0}$ = 49.2(7) GPa and its' pressure derivative, $(\partial K/\partial p)_T = K'$ = 4.89(22). This value of the ambient unit cell volume from the fitted EoS corresponds to some 99.8 % of that obtained independently at ID31. The pressure dependence of the lattice parameters, where $d^3 = a^3$, b^3 and c^3, was described by fitting a parametric form of the EoS to the weighted *p*, d^3 data obtained via Rietveld refinement. Using 2nd-order EoS to compare and describe the distinctly different behaviour of the three axes, already evident from Figure 7, we obtain: fitted a_0 = 17.8792(11) Å, $K_{T,0}(a)$ = 65.9(3) GPa; fitted b_0 = 17.8764(25) Å, $K_{T,0}(b)$ = 54.0(5) GPa and fitted c_0 = 7.9279(14) Å, $K_{T,0}(c)$ = 41.46(28) GPa. These moduli are in ratios of 100 %: 82 %: 63 %.

Due to the pseudotetragonal metrics of the TTB structure, the *Ccc*2 structure might be expected to exhibit different magnitudes of compression normal to- and parallel to the *c*-axis, which is the case. What is more significant here is that the orthorhombic symmetry is clearly reflected even in-plane, more than the closeness of lattice parameters might imply.

However, in spite of these large differences in moduli, any increase in in-plane anisotropy with pressure is limited by the curvature of the EoS determined. A description for this phenomenon is obtained from fitting a weighted 3rd-order EoS to the *p*, d^3 data: due to the pressure evolution of the axial K (d) and K' (d) values, the maximum difference in relative compression is to be observed along *x* and *y* directions between 13-18 GPa (a/a_0 = 0.944, b/b_0 = 0.937, at 16 GPa). At 32-36 GPa, the same effect results in essentially equal in-plane relative compressions (of ~0.902) and moduli (of ~198 GPa). The *b*-axis is determined to become stiffer than the *a*-axis, due to a higher $K'(b)$ = 4.2 *cf.* $K'(a)$ = 3.3, e.g. at 36 GPa. For comparison, the compression along the *c*-axis is calculated to reach 0.88, $K(c)$ = 192 GPa and $K'(c)$ = 3.64 at 36 GPa.

Therefore, for the *Ccc*2 structure under load, the plane-normal anisotropy only accelerates with pressure, whereas the pressure variation of the in-plane moduli predicts maximum divergence in axial compressions at 16 GPa and nil at double this pressure. In the absence of a first-order transition, a tetragonal metric is not expected again before pressures in excess of 65 GPa.

Magnetic properties

The molar magnetic susceptibility, χ_M, of $KMnCrF_6$, measured as

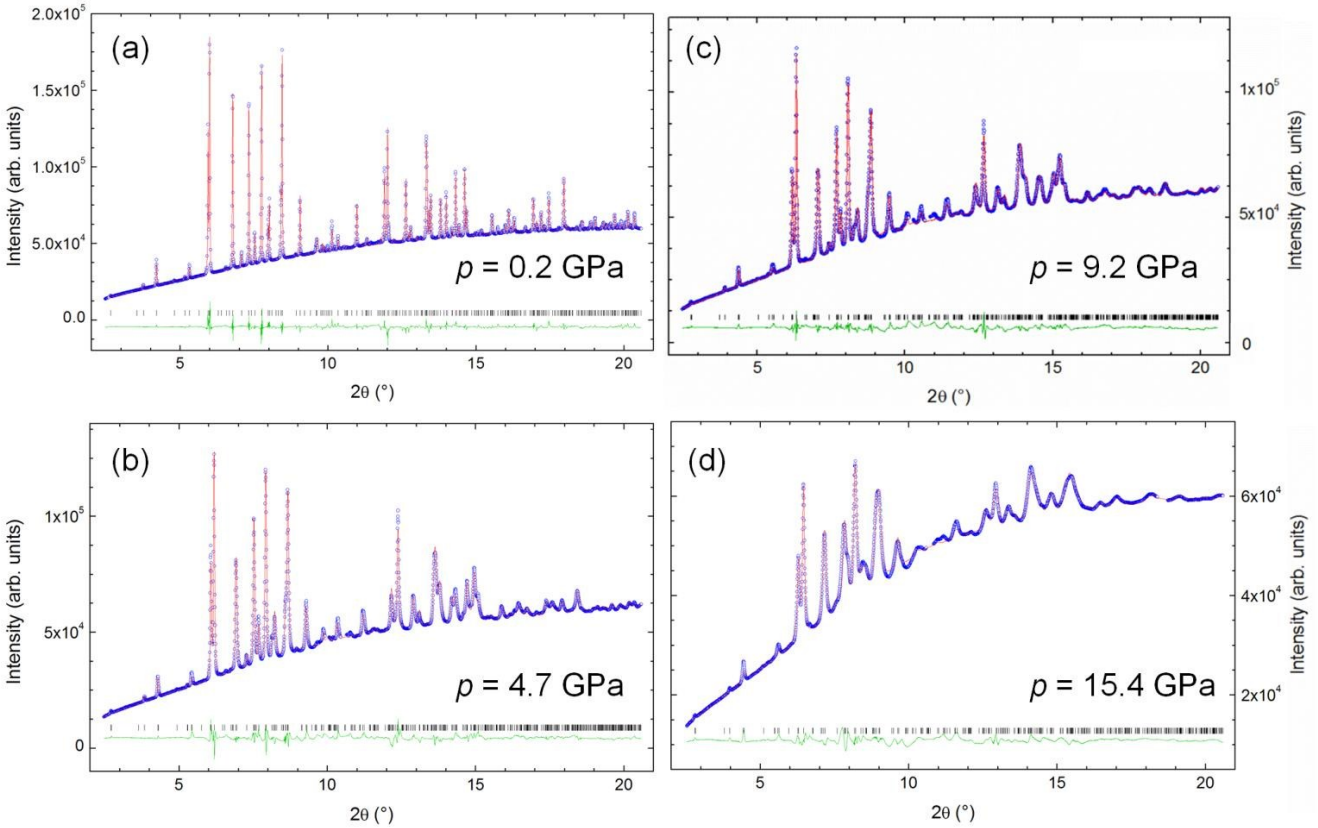

Fig. 6 Observed (open blue circles), calculated (red line) and difference (green line) high-pressure synchrotron diffraction Rietveld profile of $KMnCrF_6$ at 300 K. (a) p = 0.2 GPa (b) p = 4.7 GPa, (c) p = 9.2 GPa, (d) p = 15.4 GPa. Refinement carried out in space group *Ccc*2. Some spikes in the diffraction profile, arising from detector errors, and any reflections coming from the gasket were excluded from the refinement.

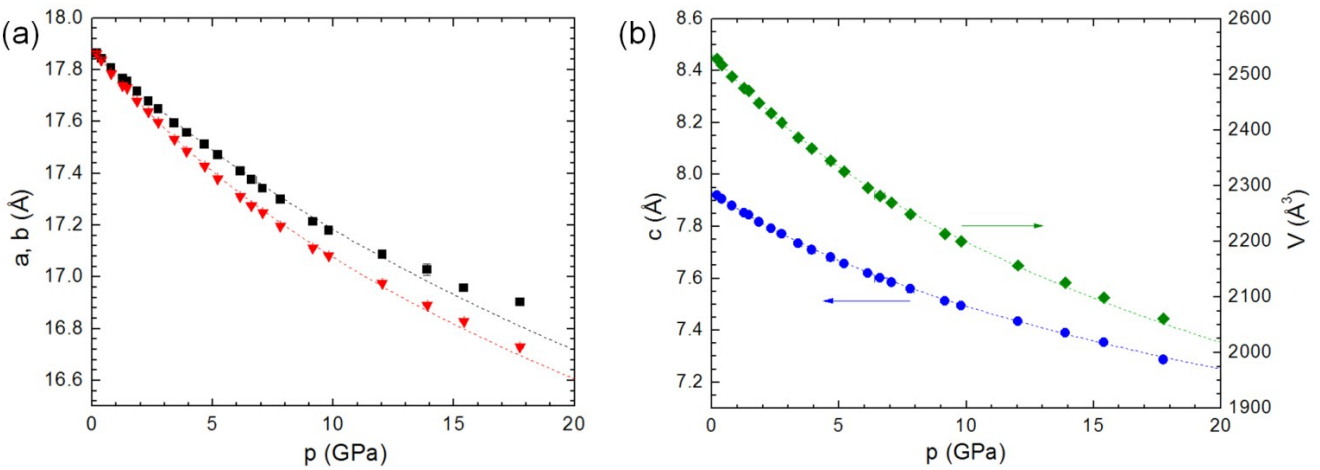

Fig. 7 Pressure evolution of (a) the basal lattice constants *a* (black squares) and *b* (red triangles), (b) the *c*-axis (blue circles) and unit cell volume (green diamonds) as obtained from Rietveld refinements of room temperature diffraction profiles collected at BL10XU. The solid line is a least-squares fit to a 3rd order Birch-Murnaghan equation of state, extended to p = 20 GPa.

a function of temperature in different applied field (0.01, 0.1 and 1 T), clearly shows a well defined increase at 23 K, providing the signature of the onset of long range magnetic ordering (Fig. 8).

In low applied fields, the zero-field cooled (ZFC) and field cooled (FC) curves bifurcate, indicating a spontaneous magnetic moment, which is saturated for $H \geq 0.1$ T. The dependence of the magnetization demonstrates that the FM component is suppressed with increasing applied field hinting at the predominance of the

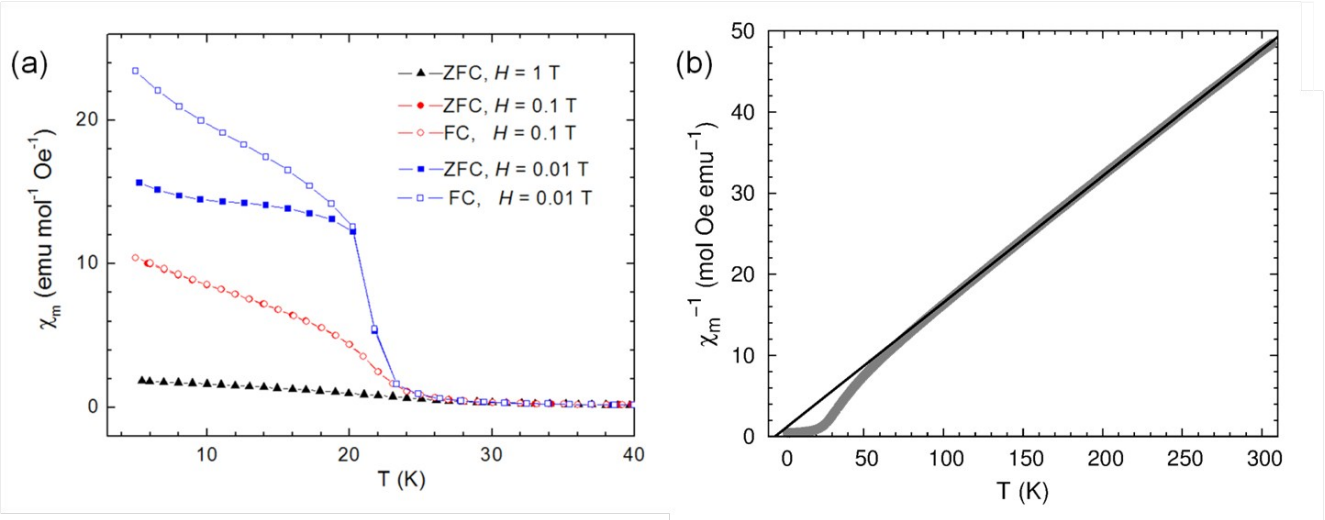

Fig. 8 Temperature dependence of the magnetic susceptibility in different applied fields H = 1 (black triangles), 0.1 (red circles) and 0.01 T (blue squares) after zero-field-cooling (open symbols) and field cooling (full symbols). (b) Temperature dependence of the inverse magnetic susceptibility χ_m^{-1}, measured in H = 1 T. At high temperatures the Curie – Weiss law is obeyed; the extrapolated fit is shown as a red line. The ferromagnetic transition temperature is determined from the $1/\chi_m$ vs. T plot as T_N = 23 K.

AF interactions. Above 100 K, the Curie-Weiss law is obeyed with a small negative Weiss temperature θ = -5.9(1) K implying the existence of (short-range) AF exchange interactions, arising from coupling of nearest-neighbour Mn-Mn and Cr-Cr pairs.[13] Curie and Weiss temperatures are consistent with those reported for the $K_xMn_xCr_{1-x}F_6$ system [13] and magnetic impurities were not visible in the high-resolution synchrotron diffraction profiles. The measured $\chi_M T$ at 300 K (6.32 emu K mol^{-1}) gives a value for the effective magnetic moment, μ_{eff} = 7.1 μ_B, which is consistent with the spin-only value that was calculated considering high-spin Mn^{2+} and Cr^{3+} ions. The magnetic hysteresis loop (M *vs* H) at 5 K shows a behaviour typical of ferrimagnets with a very small coercive field of ~ 0.0050 T and an almost saturated moment of 3.76 μ_B per formula unit at 1 T (Fig. S2). Using simple geometrical consideration and number of super-exchange pathways the overall magnetic behaviour could be estimated in accordance with the Goodenough-Kanamori rules.[28] If we satisfy the maximum number of the nearest-neighbour interactions in order of their strength – *i.e.* AF interactions between pairs of Mn^{2+} - Mn^{2+} (d^5-d^5) and Cr^{3+} - Cr^{3+} (d^3-d^3), then FM interactions of the pairs Mn^{2+} - Cr^{3+} (d^5-d^3) – the resulting model points toward a ferromagnetic behaviour resulting from the predominance of Mn^{2+} – Cr^{3+} interactions.[13] In this scenario, the appearance of ferrimagnetic properties and negative Weiss temperature is most probably connected to the high degree of frustration arising from competing AF interactions around the triangular **C** sites.

Discussion

The structural and magnetic properties of TTB fluorides have not been studied in much detail despite their evident similarities with the ferroelectric niobates and their potential multiferroic behaviour. The only exception is the series $K_xFe^{2+}{}_xFe^{3+}{}_{1-x}F_3$ ($0.6 < x < 0.5$) which has been subject of a number of papers since the late 80's when Abrahams employed his structural criteria and predicted a paraelectric-ferroelectic transition at T_C = 535 K for $K_{0.6}FeF_3$.[22] Subsequent heat-capacity and dielectric permittivity measurements provided experimental confirmation of Abraham's prediction and placed the transition at T_C = 490 K.[29] Examination of single crystals of $K_{0.6}FeF_3$ in polarised light indicated the loss of ferroelastic domains at T_C = 490(10) K.[29] This suggested a symmetry change from *mm*2 – 4/*mmm* connected to Fe^{2+}/Fe^{3+} order – disorder transition. More recently, Fabbrici *et al.* investigated the structure of $K_{0.53}FeF_3$ by single crystal and electron diffraction at room temperature.[30] It was determined that the underlying unit cell is tetragonal *P*4*bm*, with $a = b \approx a_{TTB} \approx 12.634(1)$ Å and $c \approx c_{TTB} \approx 3.9515(3)$ Å. The modulation satellites observed at room temperature were connected to the cooperative tilting of the FeF_6 octahedra, which gives rise to a ferroelastic superstructure (FES). In analogy with BNN, the FES phase was described as orthorhombic *Bbm*2, with $a \approx 2\cdot\sqrt{2}\cdot a_{TTB} \approx 35.7$ Å, $b \approx \sqrt{2}\cdot a_{TTB} \approx 17.9$ Å, $c \approx 2\cdot c_{TTB} \approx 7.9$ Å. In addition, the presence of satellite peaks that could be indexed considering a TTB cell with doubled c-axis ($a_{COS} \approx b_{COS} \approx a_{TTB} \approx$ 12 Å, $c_{COS} \approx 2\cdot c_{TTB} \approx 8$ Å), was related to a charge ordered superstructure (COS, space group $P4_2bc$). The FES and the COS structures, arising from tilt modulations and charge order respectively, seem to be independent from each other given that they each display a different periodicity relative to the fundamental TTB cell.

Increasing the potassium content to a composition of $K_{0.6}FeF_3$ leads to the stabilization of a different charge-ordered structure.[31] The COS cell is then orthorhombic with symmetry *Pba*2, where Fe^{3+} and Fe^{2+} alternate along the c-axis on the extra-perovskite sites (2*b*) and around the perovskite cage (4*c* sites) at z = 0.25. Those around the 4*c* site at z = 0.75, are statistically disordered (and occupied by nominal $Fe^{2.5+}$). Three different structural transitions occur with decreasing temperature: (i) T→O at 570 K, (ii) charge-ordering transition at 490 K and (iii) orthorhombic to monoclinic at 290 K. The monoclinic distortion was related to a FES superstructure $a_{FES} \approx 2\cdot\sqrt{2}\cdot a_{TTB} \approx 35.9$ Å, $b_{FES} \approx 2\cdot c_{TTB} \approx$

8 Å, $c_{FES} \approx \sqrt{2} \cdot a_{TTB} \approx 17.9$ Å, $\beta \approx 90.4°$.[31]

Very little is known on the structural behaviour of other TTB fluorides with mixed transition metals. Electron diffraction patterns of $K_{0.6}Mn_{0.6}Fe_{0.4}F_3$ exhibited satellite peaks related to ferroelastic and charge-ordered structures but there has been no further confirmation from diffraction experiments.[30]

Our high-resolution powder diffraction experiments on the related TTB fluoride $KMnCrF_6$, showed the presence of superlattice peaks with indexes (*hkl*, l = ½) throughout the measured temperature range (T = 5 – 950 K). The observation of these reflections clearly demonstrate the doubling of the *c*-axis with respect to the fundamental TTB cell arising from the ordering of Mn^{2+} and Cr^{3+} around the perovskite cage. At high temperatures (T > 400 K) the structure of $KMnCrF_6$ is tetragonal with symmetry $P4_2/mbc$. The space-group assignment was driven by the very small values of the atomic displacements along the *c*-axis, $d(z)$, which would not justify a description in the lower symmetry polar variant $P4_2bc$. Analysis of the bond distances give a clear indication of the ionically ordered pattern around the perovskite cage, while the extra-perovskite site is statistically occupied by the divalent and trivalent cations.

On cooling (T < 400 K) a phase transition occurs to an orthorhombically distorted structure with symmetry *Ccc*2, linked to the cooperative tilting of the MF_6 octahedra. The atomic displacements are large enough to support the acentric symmetry. One of the main differences between the orthorhombic *Ccc*2 and the tetragonal $P4_2bc$ model previously used to describe related systems is that the former allows additional ordering of the trivalent and divalent cations on the extra-perovskite sites. However, analysis of the bond distances relative to the transition metals occupying the extra-perovskite sites does not support such an ordered arrangement. It indicates statistical disorder, giving rise to an overall ionic order motif identical to that observed in the high temperature phase (T > 400 K). The orthorhombic structure is very robust and no further phase transitions are observed on cooling down to 5 K or with increasing pressures up to 18 GPa.

Is it important to mention that the orthorhombically distorted cell established for $KMnCrF_6$ is closely related to the average structure adopted by BNN at room temperature ($a \approx \sqrt{2} \cdot a_{TTB} \approx$ 17.62 Å, $b \approx \sqrt{2} \cdot a_{TTB} \approx 17.59$ Å, $c \approx c_{TTB} \approx 4.00$ Å ; space group *Cmm*2).[4] It is well known that due to octahedral tilt modulations, the real structure of BNN is a quasi-commensurate orthorhombic ferroelastic phase similar to the FES superstructure previously discussed for $K_{0.53}FeF_3$ and $K_{0.6}FeF_3$.[5,31]

The average structure of BNN describes well the off-centring of the Nb^{5+} ions, which has been interpreted in term of strong hybridization between empty Nb *d* and O 2*p* orbitals. This ferroelectric displacement is discouraged if the *d* orbitals of the transition metals are not empty. Despite the d^5 and d^3 electronic configuration, the values of the transition metal displacements obtained for $KMnCrF_6$ at room temperature are comparable to those reported for BNN (Fig. S3).[5] The *M*-F interactions are much more ionic than the *M*-O and we can expect weaker hybridization. It follows that the d^0 criterion for polar distortion applicable for oxides does not hold for fluorides taking into account the higher degree of Coulombic interactions.

In addition, the orthorhombic strain parameters of the two systems are of the order of 10^{-3} implying that interchange of the *a*- and *b*-axis of $KMnCrF_6$ could also give rise to ferroelastic domains and the stabilization of a commensurate or quasi-commensurate FES superstructure. Electron or single-crystal diffraction experiments are necessary to observe reflections relative to the FES superstructure. However, we recall that such reflections were observed at room temperature for the related $K_{0.6}Mn_{0.6}Fe_{0.4}F_3$. The main difference between the average orthorhombically distorted phases of $KMnCrF_6$ and BNN is that the former shows doubling of the *c*-axis due the ionic ordering around the perovskite cage.

Also the temperature evolution of the *c* lattice parameter shows a clear anomaly at T_S. This is a signature of octahedral distortion that becomes more pronounced on cooling. We stress that the experimental transition temperature is in very good agreement with the value calculated purely from atomic displacements.

As discussed above, the structural behaviour observed for $KMnCrF_6$ shows many similarities and identical phenomenology with other ferroelectric TTB oxides/fluorides. It is therefore very likely that the T→O structural change in $KMnCrF_6$ is linked to a paraelectric/ paraelastic – ferroelectric/ ferroelastic transition. We recall here that ferroelectricity in other fluorides has been also explained in terms of purely size effects and geometric constrains imposed by the underlying crystal structure. For instance, first principle calculations on $BaMnF_4$ have shown that the origin of ferroelectricity is linked to rotations of the fluorine octahedra and displacements of the Ba cations and no charge transfer occurs between anions and cations.[32]

In addition to ferroelectricity, the TTB fluoride $KMnCrF_6$ displays long range ferrimagnetic order below 23 K. This is in agreement with the behaviour reported for $KMnFeF_6$ and $K_{0.6}FeF_3$, which have been both described as strongly coupled magnetoelectric materials.[9,32] As the transition metal sublattice is simultaneously responsible for ferroelectricity and magnetism, an interplay between these ordering parameters is very likely and can be considered as a general feature of multiferroic TTB fluorides. Direct evidence for the ferroelectric properties of $KMnCrF_6$ could be obtained by measurement of the dielectric susceptibility or second harmonic generation; the former has been attempted a number of times unsuccessfully on powder specimens most probably due to the difficulties in obtaining well compacted samples. While further measurements are needed for a full characterization, our results clearly demonstrate that $KMnCrF_6$ possess all the ingredients to display strongly coupled multiferroic behaviour. It would be particularly important to understand if the full ionic order possible in the orthorhombic *Ccc*2 structure is actually realized and its influence on the ferroelectric properties. Neutron powder diffraction and permittivity measurements are planned to address these issues.

Conclusions

In this work we have shown that the TTB fluoride $KMnCrF_6$ undergoes a subtle structural phase change at 400 K that can be taken as signature of a paraelectric/ paraleastic – ferroelectric/ ferroelastic transition. High-resolution synchrotron X-ray powder diffraction was employed to investigate this transition. Above 400 K, $KMnCrF_6$ adopts a centrosymmetric tetragonal structure characterized by regular octahedra and partial ionic order.

Cooling below 400 K induces a phase change to a polar orthorhombic structure. The lattice parameter changes and atomic displacements are large enough to justify the space-group assignment and are comparable to those reported for other TTB ferroelectrics. The structural change is driven by the apical displacement of Mn/Cr ions and the cooperative tilting of the MF_6 octahedra while it has no apparent influence on the ionic-order pattern. The room temperature orthorhombic phase is robust upon cooling to 5 K and under application of high pressures up to 18 GPa. It is plausible to think that the obtained orthorhombic model describes the fundamental averaged structure in analogy with what has been reported for related systems such as BNN and $K_{0.53}FeF_3$.

Magnetic measurements on $KMnCrF_6$ have confirmed the onset of a long range magnetic transition to a frustrated ferrimagnetic state below 23 K. The coupling of ferroelectricity, and ferrimagnetism is therefore expected at low temperatures, making $KMnCrF_6$ a promising candidate to display magnetoelectric properties. These results open the way to further investigations of the structural phase diagrams of related TTB fluorides where changing the chemical nature of the transition metals could results in a fine-tuning of the interplay among the many ferroic ordering parameters.

Acknowledgement

We would like to thank the ESRF for provision of beamtime and the Norges forsknigsråd (Project 214260) for financial support to SM.

Notes and references

[*] *E-mail: drathen@esrf.fr*

[a] *School of Chemistry, University of Edinburgh, King's Buildings, West Mains Road, Edinburgh, EH9 3JJ, UK.*

[b] *Department of Chemistry, University of Oslo, P.O. Box 1033 Blindern, N-0315 Oslo, Norway.*

[c] *European Synchrotron Radiation Facility, 71 Avenue des Martyrs, 38000 Grenoble, France.*

[d] *SPring-8/ JASRI, 1-1-1 Kouto, Mikaduki-chom Sayo-gun, Hyogo, 679-5198, Japan.*

[‡] *Present address: Institute of Physics, Chinese Academy of Science, Beijing, China.*

[§] *Present address: Johnson Matthey Technology Centre, Savannah, GA, USA.*

† Electronic Supplementary Information (ESI) available: Atomic displacements at 300 K and 423 K; Rietveld refinement at 5 K, magnetic hysteresis loop at 5 K, Rietveld refinement results at 423 K in space group $P4_2bc$; A X-ray crystallographic file (CIF) of the *Ccc*2 structure at 300 K and 5 K as well as the $P4_2/mbc$ structure at 423 K. See DOI: 10.1039/b000000x/

.

1 Mangéli, A. *Arkiv foer Kemi*, 1949, **1**, 269.
2 Simon, A.; Ravez, J.; *C. R. Chimie*, 2006, **9**, 1268.
3 Geusic, J. E.; Levinstein, H. J.; Singh, S.; Smith, R. G.; Van Uitert, L. G; *Appl. Phys. Lett*. 1968, **12**, 306.
4 Jamieson, A.; Bernstein, *J. Chem. Phys.* 1969, **50**, 4352.
5 Labbe, P.; Leligny, H.; Raveau, B.; Schneck, J.; Toledano, J.C. *Journal of Physics: Condensed Matter*, 1990, **2**, 25.
6 Scott, J.; Hayward, S.; Miyake, M. *J.Phys.: Condens. Matter* 2005, **17**, 5911.
7 Filipic, C.; Kutnjak, Z.; Lortz, R.; Torres-Pardo, A.; Dawber, M.; Scott, J.F. *J.Phys.: Condens. Matter* 2007, **19**, 236206.
8 Ravez, J.; Abrahams, S.C.; Mercier, A.M.; Rabardel, L.; de Pape, R. *J. Appl. Phys.*, 1990, **67**, 3.
9 Nénert, G.; Palstra, T.T.M. *J. Phys.: Condens. Matter* 2007, **19**, 406213.
10 Banks, E.; Nakajima, S.; Williams, G.J.B. *Acta Crystallogr. Sect.B*, 1979, **35**, 46-49.
11 Banks, E.; Shone, M.; Williamson, R.F.; Boo, W.O.J. *Inorg. Chem.*, 1983, **22**, (22), 3339-3342.
12 Lacorre, P.; Pannetier, J.; Ferey, G. *J. Magn. Magn. Mater.*, 1991, **94**, 331-336.
13 Banks, E.; Shone, M.; Hong, Y.S.; Williamson, R.F.; Boo, W.O.J. *Inorg. Chem.*, 1982, **21**, 3894-3897.
14 Hong, Y.S.; Boo, W.O.J.; Mattern, D.L. *J. Solid State Chem.*, 2010, **183**, 1805-1810.
15 Giri, S.; Ghoshray, K.; Ghosray, A. *Solid State Commun.*, 1995, **93**, (6), 493-495.
16 Scott, J. F., *NPG Asia Materials*, 2013, **5**, e72.
17 Billinge, S.; Difrancesco, R.; Kwei, G.; Neumeier, J.; Thompson, J. *Phys. Rev.Lett.*, 1996, **77**, 715.
18 Larson, A.C.; v.Dreele, R.B. Los Alamos National Laboratory Report, 2004, LAUR 86-748, 1-231.
19 Toby, B. *J. Appl. Crystallogr.*, 2001, **34**, 210.
20 Brese, N.E.; O'Keefe, M., *Acta Crystallogr. Sect. B*, 1991, **47**, 192-197
21 Brown, I.D.; Altermatt, D., *Acta Crystallogr. Sect. B*, 1985, **41**, 244-247.
22 Abrahams, S.C. *Acta Crystallogr. Sect. B*, 1989, **45**, 228-232.
23 Abrahams, S.C. *Acta Crystallogr. Sect. B*, 1996, **52**, 790-805.
24 Abrahams, S.C. *Acta Crystallogr. Sect. B*, 1988, **44**, 585-595.
25 Kroumova, E.; Aroyo, M.; Perez-Mato, J. *Acta Crystallogr. Sect. B*, 2002, **58**, 921.
26 Capillas, C.; Tasci, E.S.; de la Flor, G.; Orobengoa, D.; Perez-Mato J.M; Aroyo, M.I. *Z. Kristallogr.- New Cryst.Struct.*, 2011, **226** (2), 186-196.
27 Angel, R.; *Rev. Mineral. Geochem.*, 2000, **41**, 35.
28 Kanamori, J. *J. Phys. Chem. Solids*, 1959, **10**, 87. Anderson, P.W. *Magnetism.* Academic, New York 1963
29 Ravez, J.A.; De Pape, R. *J. Appl. Phys.*, 1989, **65**, 4.
30 Fabbrici, S.; Montanari, E.; Righi, L. ; Calestani, G. ; Migliori, A. *Chem. Mater.* 2004, **16**, 3007-3019. 31 Mezzadri, F.; Fabbrici, S.; Montanari, E.; Righi, L. ; Calestani, G. ; Gilioli, E. ; Bolzoni, F. ; Migliori, A. *Phys. Rev. B: Condens. Matter Mater. Phys.*, 2008, **78**, 064111.
32 Ederer, C.; Spaldin, N.A.; *Phys. Rev. B: Condens. Matter Mater. Phys.*, 2006, **74**, 024102.

Structural transition in $KMnCrF_6$ – a chemically ordered magnetic ferroelectric.

Christina Drathen,*[a,c] Takeshi Nakagawa,[b‡] Wilson A. Crichton,[c] Adrian H. Hill,[c§] Yasuo Ohishi [d] and Serena Margadonna[b]

Graphical abstract for the contents page:

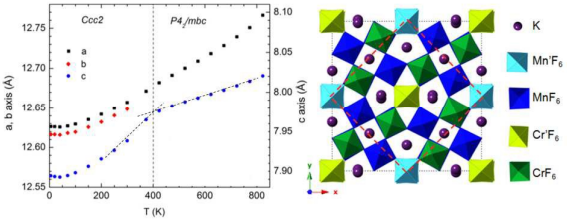

Text:

Emergence of an orthorhombic phase at room temperature suggests this tetragonal tungsten bronze fluoride as potential multiferroic material.